
Research Article: New Research | Disorders of the Nervous System

A HIF1a-dependent pro-oxidant state disrupts synaptic plasticity and impairs spatial memory in response to intermittent hypoxia

<https://doi.org/10.1523/ENEURO.0024-20.2020>

Cite as: eNeuro 2020; 10.1523/ENEURO.0024-20.2020

Received: 24 January 2020

Revised: 30 April 2020

Accepted: 15 May 2020

This Early Release article has been peer-reviewed and accepted, but has not been through the composition and copyediting processes. The final version may differ slightly in style or formatting and will contain links to any extended data.

Alerts: Sign up at www.eneuro.org/alerts to receive customized email alerts when the fully formatted version of this article is published.

Copyright © 2020 Arias-Cavieres et al.

This is an open-access article distributed under the terms of the Creative Commons Attribution 4.0 International license, which permits unrestricted use, distribution and reproduction in any medium provided that the original work is properly attributed.

1 **Title:** A HIF1a-dependent pro-oxidant state disrupts synaptic plasticity and impairs spatial memory in response
2 to intermittent hypoxia

3
4 **Abbreviated Title:** HIF1a and hippocampal neurophysiology

5
6 **Authorship:** Alejandra Arias-Cavieres¹, Maggie A. Khuu³, Chinwendu U. Nwakudu³, Jasmine E. Barnard³,
7 Gokhan Dalgin⁴, Alfredo J. Garcia III^{1,2,3}

8
9 **Affiliations:**

10 ¹Institute for Integrative Physiology, The University of Chicago;

11 ²Grossman Institute for Neuroscience, Quantitative Biology & Human Behavior, The University of Chicago;

12 ³Department of Medicine, Section of Emergency Medicine, The University of Chicago;

13 ⁴Department of Medicine Section of Adult and Pediatric Endocrinology, Diabetes, and Metabolism, The
14 University of Chicago.

15
16
17 **Keywords:** sleep apnea, NMDA receptor, Oxidative Stress

18
19 **Author Contributions:** AJG conceived and designed experiments; AAC, MAK, JEB, CUN, GD and AJG
20 performed experiments, and conducted analyses; AAC, MAK, and AJG wrote and/or revised the manuscript;
21 AJG provided unpublished reagents and analytic tools.

22 **Correspondence:** Alfredo J. Garcia III, ajgarcia3@uchicago.edu

23 **Figure Number:** 6

Abstract: 203 words

24 **Table Number:** 1

Significance Statement: 66 words

25 **Introduction:** 347 words

Discussion: 968 words

26 **Acknowledgements:** The authors wish to thank Dr. Nanduri Prabhakar and Dr. Gregg Semenza for the
27 provision of the HIF1a^{+/-} mouse line. The authors would also like to thank Dr. N. Prabhakar for the sound
28 advice throughout the course of the study and the preparation of the manuscript. This article was first published
29 as a preprint: A Arias-Cavieres, MA Khuu, CU Nwakudu, JE Barnard, G Dalgin, AJ Garcia III (2019). *A role for*
30 *Hypoxia Inducible Factor 1a (HIF1a) to intermittent hypoxia-dependent changes in spatial memory and*
31 *synaptic plasticity*. bioRxiv. <https://doi.org/10.1101/595975>.

32 **Conflict of Interest:** The authors have no conflicts of interests related to this study.

33 **Funding Sources:** This work was supported by NIH PO 1 HL 144454 (AJG), NIH R01 NS10742101 (AJG), a
34 grant from The BSD Office of Diversity & Inclusion at The University of Chicago (AJG). GD was also
35 supported by The University of Chicago Diabetes Research Center (P30 DK020595).

39 **Abstract:**

40 Sleep apnea causes cognitive deficits and is associated with several neurologic diseases. Intermittent hypoxia
41 (IH) is recognized as a principal mediator of pathophysiology associated with sleep apnea, yet the basis by
42 which IH contributes to impaired cognition remains poorly defined. Using a mouse model exposed to IH, this
43 study examines how the transcription factor, Hypoxia Inducible Factor 1a (HIF1a), contributes to disrupted
44 synaptic physiology and spatial memory. In wildtype mice, impaired performance in the Barnes maze caused
45 by IH coincided with a loss of NMDA receptor dependent Long Term Potentiation (LTP) in area CA1 and
46 increased nuclear HIF1a within the hippocampus. IH-dependent HIF1a signaling caused a two-fold increase in
47 expression of the reactive oxygen species generating enzyme NADPH oxidase 4 (NOX4). These changes
48 promoted a pro-oxidant state and the downregulation of GLUN1 within the hippocampus. The IH-dependent
49 effects were not present in either mice heterozygous for *Hif1a* (HIF1a^{+/-}) or wild type mice treated with the
50 antioxidant MnTMPyP. Our findings indicate that HIF1a dependent changes in redox state are central to the
51 mechanism by which IH disrupts hippocampal synaptic plasticity and impairs spatial memory. This mechanism
52 may enhance the vulnerability for cognitive deficit and lower the threshold for neurologic diseases associated
53 untreated sleep apnea.

54 **Significance:**

55 Sleep apnea is associated with cognitive decline and neurological disease. Intermittent hypoxia, a hallmark
56 consequence of sleep apnea, yet the mechanisms by which IH affects cognition is poorly understood. We
57 show that a pro-oxidant state produced by HIF1a is a central factor causing IH-dependent impairment to spatial
58 memory and synaptic plasticity. This work identifies potential targets for intervention in mitigating cognitive
59 decline associated with sleep apnea.

60

61 **Introduction:**

62 The hippocampus is widely regarded for its importance in learning and memory, and is frequently identified as
63 a brain structure impacted by sleep apnea (Sforza et al., 2016; Cha et al., 2017; Macey et al., 2018; Song et
64 al., 2018). As cognitive decline is a recognized comorbidity of sleep apnea (Wallace and Bucks, 2013; Varga et
65 al., 2014; Gildeh et al., 2016; Devita et al., 2017a; Devita et al., 2017b; Leng et al., 2017), changes to
66 hippocampal physiology may have a significant role in disrupting cognition. Intermittent hypoxia (IH) is a
67 hallmark of the sleep apnea and impairs spatial learning and memory (Row et al., 2002; Gozal et al., 2003).
68 These impairments coincide with weakened synaptic plasticity in area CA1 of the hippocampus (Goldbart et
69 al., 2003; Payne et al., 2004; Xie et al., 2010; Zhang et al., 2012; Wall et al., 2014) and the production of
70 oxidative stress in the brain (Nair et al., 2011; Chou et al., 2013). Impaired synaptic plasticity and oxidative
71 stress have been implicated in causing IH-dependent deficits to cognition, but the mechanistic basis by which
72 IH impairs learning and memory remains elusive.

73 The transcription factor, hypoxia inducible factor 1a (HIF1a) is a critical mediator of cellular adaptations to
74 hypoxia, and is capable of promoting the generation of reactive oxygen species (ROS) that can lead to
75 oxidative stress (Semenza and Prabhakar, 2015). IH increases HIF1a in the hippocampal formation (Chou et
76 al., 2013; Wall et al., 2014). However, the role of IH-dependent HIF1a signaling on IH-dependent changes to
77 the neurophysiological processes underlying cognition remains poorly understood. HIF1a signaling may have
78 an important protective pro-survival role in the brain preserving function in response to the hypoxia
79 experienced during IH. Alternatively, HIF1a may serve as a pro-oxidant transcription factor leading to oxidative
80 stress and impaired neurophysiology. Here, we seek to resolve the role of HIF1a in IH-dependent changes to
81 cognition and the synaptic plasticity. Our experiments demonstrate that enhanced HIF1a signaling promotes a
82 pro-oxidant condition that impairs N-Methyl-D-Aspartate receptor (NMDAR) dependent synaptic plasticity at the
83 local circuit level and contributes deficits in spatial memory.

84

85 **Methods:**

86 **Study Approval.** In accordance with National Institutes of Health guidelines, all animal procedures were
87 performed in accordance with the [Author University] animal care committee's regulations.

88 **Animals.** Animals were housed in AAALAC-approved facilities with a 12 hour/12 hour light-dark cycle and
89 given ad libitum access to food and water. Experiments were performed on wildtype mice and HIF1a^{+/-} (Iyer et
90 al., 1998; Peng et al., 2006) from both sexes (P50 to P80). Unless explicitly stated, no sex-based differences
91 were observed throughout the experiments conducted. All animals were maintained on a C57BL/6 background.
92 Automated genotyping was performed independently by a commercial service (Transnetyx Inc).

93 **Intermittent hypoxia (IH) exposure.** Male and female mice were exposed to chronic intermittent hypoxia for
94 ten consecutive days (IH₁₀). In brief, as previously described (Peng and Prabhakar, 2003), the IH₁₀ paradigm
95 was performed in a special chamber during the light cycle and lasted 8 hours per day (i.e., 80 intermittent
96 hypoxia cycles/day). A single hypoxic cycle was achieved by flowing 100% N₂ into the chamber for
97 approximately 60s (nadir O₂ reached 4.5±1.5% and followed immediately by an air break (~21% O₂; 300s).

98 In a subset of animals used for behavioral experiments, manganese (III) tetrakis(1-methyl-4-pyridyl) porphyrin
99 (MnTMPyP, Enzo Life Sciences, CAT #: ALX-430-070), was administered via intraperitoneal injection at the
100 beginning of each day prior to exposure to IH. Previous reports have indicated that dose of MnTMPyP at
101 either 5mg/kg (Peng et al., 2006) or 15mg/kg (Khuu et al., 2019) can mitigate the effects of IH in the nervous
102 system. Therefore, the smaller dose (5 mg/kg, n=9 mice) and the larger dose (15mg/kg, n=3 mice) were used
103 but no differences were evident between dosage groups; and therefore, the data at the two concentrations
104 were pooled.

105 **Barnes maze.** The Barnes maze was performed using a custom made opaque white circular acrylic platform
106 (92.4 cm in diameter) with 20 equidistant holes (5.08 cm in diameter and 2.54 cm from the edge). The platform
107 was elevated (30 cm from the floor) ground and surrounded by four identical walls (27.94 cm high). By default,
108 each hole was closed with a fixed piece of opaque acrylic that could be removed to lead to a dark exit box.
109 Lighting was achieved through diffuse overhead fluorescent lighting such that all holes were equally lit. An
110 overhead camera was suspended above the maze allowing for video tracking. Data collection and *posthoc*
111 analysis was performed using CinePlex Video Tracking System (Plexon, Dallas, TX).

112 As previously described (Christakis et al., 2012), the task was performed using a four-day protocol consisting
113 of one training trial per day for three consecutive days and a probe trial on the fourth day. Barnes Maze began
114 on the seventh day of IH₁₀ exposure with respective controls run at the same time. In IH mice, all training trials

115 and the probe trial were conducted prior to IH exposure on days 7 to 10. For the training trials, all, but one of
116 the holes (exit hole), were closed. Closed holes were defined as false exits in the training and probe trials. An
117 exit box with a small ramp was placed directly underneath the exit hole. Animals were given a maximum of six
118 minutes to locate the exit. If the mouse found and entered the exit before the six-minute mark, the trial ended.
119 The time of exit was reported as total latency for the trial. If the mouse was unable to locate the exit by six
120 minutes, they were gently guided to the exit and total latency for the trial was reported as 360 sec. At end of
121 each trials, the mouse was promptly returned to its home cage. During the probe trial, all holes were closed,
122 and the animal was given six minutes to explore the maze. Latency to initial entry and distance to initial entry
123 into the exit zone were reported. All subjects entered the exit zone during the probe trial. The total number of
124 entries for each false exit and the exit were recorded and used to calculate entry probability.

125 Entry probability for each false exit and the exit zone during the probe trial was calculated by the following:

$$126 \quad EP_n = 100\% \times \frac{x_n}{x_{total}}$$

127 where EP_n = entry probability for the exit zone; x_n = number of entries into hole n; and x_{total} = sum of entries into
128 exit zone and false exits .

129 The entire arena was sanitized in-between trials. Following the end of behavioral testing, IH animals were
130 immediately placed into the IH chamber for exposure.

131

132 **Slice Preparation.** As previously described (Khuu et al., 2019), acute coronal hippocampal slices were
133 prepared from mice unexposed to intermittent hypoxia or from mice exposed to IH for ten days. Tissue harvest
134 occurred within one to two days following IH₁₀. Mice were anesthetized with isoflurane and euthanized via rapid
135 decapitation. The cerebrum was immediately harvested and blocked, rinsed with cold artificial cerebrospinal
136 fluid (aCSF), and mounted for vibratome sectioning. The mounted brain tissue was submerged in aCSF (4°C;
137 equilibrated with 95% O₂, 5% CO₂) and coronal cortico-hippocampal brain slices (350 μm thick) were prepared.
138 Slices were then immediately transferred into a holding chamber containing aCSF equilibrated with 95% O₂,
139 5% CO₂ (at 20.5±1°C). Slices were allowed to recover for a minimum of one hour prior to recording and used

140 up to eight hours following tissue harvest. The composition of aCSF (in mM): 118 NaCl, 10 glucose, 20
141 sucrose, 25 NaHCO₃, 3.0 KCl, 1.5 CaCl₂, 1.0 NaH₂PO₄ and 1.0 MgCl₂.

142 **Extracellular recording of the field excitatory postsynaptic potential (fEPSP).** For electrophysiological
143 recordings, slices were transferred to a recording chamber with recirculating aCSF (30.5±1°C, equilibrated with
144 95% O₂ and 5% CO₂) and allowed 15 min to acclimate to the recording environment. The fEPSP in the CA1
145 was evoked by electrical stimulation. The stimulation electrode was positioned in Schaffer Collateral and the
146 recording electrode (1-2 MΩ) was placed into the stratum radiatum of the CA1. The intensity of the electrical
147 current (100-400 μA; 0.1-0.2 ms duration) was set to the minimum amount of current required to generate
148 ~50% of the maximal initial slope (m_i) of the fEPSP. The current stimulus used to examine the unpotentiated
149 fEPSP was evoked at 700μA (a stimulus intensity that evoked the maximal fEPSP amplitude in aCSF for all
150 slices) and examined in aCSF, Mg²⁺ free aCSF, and Mg²⁺ free aCSF with 20 μM AP5 (Sigma-Aldrich, MN).
151 The composition of Mg²⁺ free aCSF (in mM): 119.5 NaCl, 10 glucose, 20 sucrose, 25 NaHCO₃, 3.0 KCl, 1.5
152 CaCl₂, 1.0 NaH₂PO₄. The NaCl was increased to 119.5 mM to keep osmolarity from changing when switching
153 from aCSF to Mg²⁺ free aCSF. The fEPSP was evoked every 20 s. After 10 min of recording the baseline
154 fEPSP, LTP was induced using high frequency stimulation (HFS) or theta burst stimulation (TBS). HFS
155 consisted four 500 ms trains of stimuli (100 Hz) given at 30 s intervals. TBS was consisted of four trains of 10
156 bursts at 5Hz, each burst was comprised of four pulses at 100 Hz. The fEPSP slope was normalized to
157 baseline values (prior to HFS).

158 All recordings were made using the Multiclamp 700B (Molecular Devices:
159 [https://www.moleculardevices.com/systems/conventional-patch-clamp/multiclamp-700b-microelectrode-](https://www.moleculardevices.com/systems/conventional-patch-clamp/multiclamp-700b-microelectrode-amplifier)
160 [amplifier](https://www.moleculardevices.com/systems/conventional-patch-clamp/multiclamp-700b-microelectrode-amplifier)). Acquisition and post hoc analyses were performed using the Axon pCLAMP10 software suite
161 (Molecular Devices: [https://www.moleculardevices.com/system/axon-conventional-patch-clamp/pclamp-11-](https://www.moleculardevices.com/system/axon-conventional-patch-clamp/pclamp-11-software-suite)
162 [software-suite](https://www.moleculardevices.com/system/axon-conventional-patch-clamp/pclamp-11-software-suite)).

163 **Western Blot.** Western blot assays were performed using entire hippocampal tissue homogenates from
164 control and IH exposed mice. Hippocampal tissue from animals exposed to IH was harvested for western blot
165 analysis approximately 12 to 16 hours following the end of the IH₁₀ protocol.

166 For quantitative analysis of HIF1a (R and D Systems Cat# AF1935, RRID:AB_355064) and Proliferating Cell
167 Nuclear Antigen (PCNA, Bethyl Cat# A300-276A, RRID:AB_263393) content. Stepwise separation of
168 cytoplasmic and nuclear protein extracts was prepared by NE-PER nuclear and cytoplasmic extraction kit
169 (Thermo Scientific, 78833) by following manufacturer instructions. Briefly, cytoplasmic fragment was obtained
170 by homogenizing tissue using a tissue grinder and then by pipetting in cytoplasmic extraction buffers. After
171 isolation of cytoplasmic fragment, the insoluble pellet that contains nuclear proteins was suspended in nuclear
172 extraction buffer and separated by centrifugation. Halt Protease Inhibitor (Thermo Scientific, 1860932) was
173 added into cytoplasmic and nuclear extraction buffers to prevent protein degradation. Analyses for HIF1a and
174 PCNA proteins were conducted by Raybiotech, Inc. (Norcross, GA), using the automated Capillary
175 Electrophoresis Immunoassay machine (WEST™, ProteinSimple Santa Clara, CA). The samples, blocking
176 reagent, wash buffer, primary antibodies, secondary antibodies, and chemiluminescent substrate were
177 dispensed into designated wells in the manufacturer provided microplate. After plate loading, the separation
178 electrophoresis and immunodetection steps took place in the capillary system and were fully automated. Auto
179 Western analysis was carried out at room temperature, and instrument default settings were used.

180 Quantitative western blot analysis for GLUN1, PSD-95, NOX4 and GAPDH were performed from hippocampal
181 homogenates homogenized using either M-PER™ (Thermo Fisher, Waltham, CA, USA) or RIPA buffer
182 (Thermo Fisher, Waltham, CA, USA) in the presence of protease and phosphatase inhibitors (Thermo Fisher,
183 Waltham, CA, USA) in cold ice. Samples were centrifuged at 14 rpm for 15 min at 4 °C and the pellet was
184 discarded. Samples were boiled for 15 min in loading buffer (Bio-Rad, Hercules, CA, USA) at 60°C before
185 loading 20-25 µg protein onto 4-20% Mini-PROTEAN TGX Stain-Free™ Protein Gels (Bio-Rad, Hercules,
186 CA, USA) and electrophoresed (120 V for 100 min) using Tris/Glycine/SDS buffer (Bio-Rad, Hercules, CA,
187 USA). Gels were transferred to PVDF membrane (Bio-Rad) using Transfer-Blot Turbo System (BIO-RAD,
188 Hercules, CA, USA). Membranes were subsequently blocked (1 hr, room temperature) with 5% non-fat milk
189 (Bio-Rad, Hercules, CA, USA) or 5% bovine serum albumin (BSA) (Sigma-Aldrich, MN, USA) in Tris buffered
190 saline (TBS) (Bio-Rad, Hercules, CA, USA). Membranes were incubated (at 4°C overnight in 5% non-fat milk
191 or BSA) under constant shaking with primary antibodies: monoclonal rabbit anti GLUN1 (1:2000, Abcam),
192 monoclonal rabbit anti-PSD-95 (1:1000, Cell signal), monoclonal rabbit anti- NOX4 (1:2000, Abcam)

193 or monoclonal mouse anti-GAPDH (1:5000, Jackson ImmunoResearch). After washing three times with TBS-
194 Tween 0.2% for 15 min, membranes were incubated (1 hr, room temperature) with the appropriate secondary
195 antibodies. Finally, membranes were washed three times with TBS-Tween 0.2 % for 15 min and
196 immunoreactive proteins were detected with enhanced chemiluminescence (ECL) reagents according to
197 manufacturer instructions (Bio-Rad, Hercules, CA, USA). Signals were captured with the ChemiDoc system
198 (Bio-Rad, Hercules, CA, USA). The IMAGE J image program (National Institutes of Health,USA) was used to
199 quantify optical band intensity.

200 **Protein Carbonyls.** Whole cell protein lysates were isolated from hippocampal tissues by using M-PER
201 mammalian protein extraction reagent (Thermo Scientific, 78501) and by adding Halt Protease Inhibitor
202 (Thermo Scientific, 1860932). Protein lysates were immediately processed or kept in -80°C until used. The
203 amount of protein carbonyls was determined using a Protein Carbonyl Colorimetric Assay Kit (Cayman
204 Chemical, Cat#10005020), per manufacturer instructions and absorbance was measured at a wavelength
205 between 360-385 nm using a plate reader. Protein content was determined using a Protein Determination Kit
206 (Cayman Chemical, Cat# 704002).

207 **Experimental Design and Statistical Analyses.** All n values are total number of animals, unless otherwise
208 noted. Statistics were performed using Origin 8 Pro (OriginLab, RRID:SCR_014212) or Prism 6 (GraphPad
209 Software; RRID:SCR_015807). Comparisons between two groups were conducted using unpaired two-tailed t
210 tests with Welch's correction. To compare three or more groups, a one-way ANOVA was performed followed
211 by *posthoc* Dunnett's test comparing experimental groups to control. Results are presented as single data
212 points from each individual experiment and/or as the mean \pm S.E.M. Significance was considered when the P-
213 value was less than 0.05. See **Table 1** for statistical information related to analyses presented in this study.

214

215 **Results:**

216 HIF1a protein content was measured in nuclear extracts prepared from wildtype mice unexposed to IH
217 (control) and exposed to ten days of IH (IH₁₀). Nuclear HIF1a was approximately two times greater in extracts
218 from IH₁₀ than control (**Figure 1A**, control n=4, IH₁₀ n=4). To determine the behavioral consequences of IH, we
219 examined spatial learning and memory by assessing performance in a Barnes maze in control (n=11) and IH₁₀

220 (n=10). During training, control and IH₁₀ exhibited progressive improvement on locating the exit zone as
221 indicated by the decrease in latency to exit over course of three training sessions and was similar between
222 groups (**Figure 1B**).

223 In the probe trial (when the exit was closed), no difference was evident between the total distance travelled
224 between control and IH₁₀ (control: 25.22 ± 1.74 m versus IH₁₀: 27.91 ± 2.21 m, P=0.35, data not shown)
225 suggesting no locomotor differences between groups. However, performance in locating the exit zone was
226 different between control and IH₁₀ as the distance to initial entry to the exit zone was greater in IH₁₀ (**Figure 1C**,
227 control: 2.60 ± 0.70 m versus IH₁₀: 10.34 ± 3.32 m, P=0.048), and a larger latency to initial entry exit zone was
228 observed in IH₁₀ (**Figure 1C**, control: 22.60 ± 6.28 sec versus IH₁₀: 117.90 ± 37.47m, P=0.034). Additionally,
229 when comparing the probability to exit zone entry, the control group consistently discriminated the location of
230 exit hole against the other holes, yet this was not apparent in IH₁₀ (**Figure 1D**; control: 15.93 ± 2.39% versus
231 IH₁₀: 6.44 ± 1.38%, P=0.0037). Together these findings indicated that wildtype animals exposed to IH have
232 increased expression of HIF1a and impairments to spatial memory.

233 Nuclear HIF1a protein content was similar between extracts from hippocampi of HIF1a^{+/-} mice unexposed to IH
234 (0-HIF1a^{+/-}) when compared to HIF1a^{+/-} mice exposed to ten days of IH (10-HIF1a^{+/-}) (**Figure 1E**, 0-HIF1a^{+/-},
235 n=4, 10-HIF1a^{+/-} n=4). In 0-HIF1a^{+/-}(n=7), and 10-HIF1a^{+/-} (n=8) performance in the Barnes maze was similar
236 over the course of the training sessions (**Figure 1F**). During the probe trial, the total distance travelled by 0-
237 HIF1a^{+/-} to 10-HIF1a^{+/-} were similar (0-HIF1a^{+/-}=19.47 ± 1.61 m, 10-HIF1a^{+/-}=22.42 ± 1.61 m; P=0.55, data not
238 shown) suggesting no locomotor differences between groups. Moreover, the distance to initial entry to the exit
239 zone (**Figure 1G**, 0-HIF1a^{+/-}=2.37 ± 0.91 m, 10-HIF1a^{+/-}=1.71 ± 0.50 m; P=0.54), latency to initial entry into the
240 exit zone (**Figure 1G**, 0-HIF1a^{+/-}=35.18 ± 12.28 sec, 10-HIF1a^{+/-}= 57.28 ± 27.08 sec; P=0.48); and the entry
241 probability into the exit zone (**Figure 1H**, 0-HIF1a^{+/-}=8.75 ± 1.38%, 10-HIF1a^{+/-}=15.51 ± 4.73%; P=0.21) for
242 0-HIF1a^{+/-} and 10-HIF1a^{+/-} were similar between both groups. These data demonstrate that in HIF1a^{+/-} mice
243 the IH-dependent increase in nuclear HIF1a protein was mitigated, and spatial memory was unaffected by IH.
244 Furthermore, these data raise the possibility that increased hippocampal nuclear HIF1a signaling causes
245 deficits to hippocampal LTP.

246 The mechanisms underlying LTP are key substrates for learning and memory. We, therefore, examined LTP
247 from area CA1 in hippocampal in brain slices from control and IH₁₀. LTP from control was consistently evoked
248 by high frequency stimulation (LTP_{HFS}; **Figure 2A** blue, n=6). NMDAr blockade with AP5 attenuated LTP_{HFS}
249 magnitude but did not prevent the occurrence of the phenomenon (**Figure 2A** green, n=5). These findings
250 demonstrated that both NMDAr-dependent and NMDAr-independent mechanisms contributed to the
251 generation of LTP_{HFS}. Following IH, LTP_{HFS} was smaller in magnitude (**Figure 2A** red, n=6) and was no longer
252 sensitive to AP5 (**Figure 2A** gold, n=5).

253 We next examined whether IH prevented another LTP evoked by theta burst stimulation (LTP_{TBS}; **Figure 2B**
254 light blue, n=5), a form of synaptic potentiation dependent on the NMDAr, as AP5 prevent LTP_{TBS} (**Figure 2B**
255 light green, n=5). Following IH, LTP_{TBS} could no longer evoked (**Figure 2B** pink, n=5).

256 In contrast to the wildtype, LTP_{HFS} was similar in 0-HIF1a^{+/-} (**Figure 2C** grey n=8) and in 10-HIF1a^{+/-} (**Figure 2C**
257 dark yellow, n=8) (**Figure 2C**). In the hippocampal brain slice, the magnitude of LTP_{TBS} was similar between 0-
258 HIF1a^{+/-} (**Figure 2D** light grey, n=6) and in 10-HIF1a^{+/-} (**Figure 2D** light yellow, n=5). Additionally, AP5
259 blocked LTP_{TBS} in the 10-HIF1a^{+/-} (**Figure 2D** light green, n=4). Together these findings suggested that IH-
260 dependent HIF1a signaling suppresses NMDAr-dependent potentiation by disrupting the NMDAr physiology.
261 To test this, we examined the contribution of the NMDAr to the unpotentiated fEPSP.

262 A fEPSP with maximal amplitude in aCSF (fEPSP_{max}) was evoked using saturating current stimulus (700μA)
263 (**Figure 3A**, black=aCSF) in control (n=6, fEPSP_{max}= -1.05 ± 0.14mV), IH₁₀ (n=7, fEPSP_{max}= -0.85 ± 0.08mV),
264 0-HIF1a^{+/-} (n=9, fEPSP_{max}= -0.941 ± 0.04mV), and 10-HIF1a^{+/-} (n=11, fEPSP_{max}= -0.90 ± 0.06mV). When
265 compared to control, no difference in fEPSP_{max} was observed from any experimental group (*data not shown*,
266 One-way ANOVA: P=0.39, F=1.035; control vs. IH₁₀: P>0.05, 95% CI of diff= -0.4960 to 0.09542; control vs.
267 0-HIF1a^{+/-}: P>0.05, 95% CI of diff= -0.3938 to 0.1665; 10-HIF1a^{+/-}: P>0.05, 95% CI of diff=-0.4219 to 0.1176).
268 Switching to Mg²⁺ free aCSF relieved the Mg²⁺ blockade of existing NMDAr and caused the fEPSP to increase
269 all groups (**Figure 3A**, blue=Mg²⁺ free). The change in fEPSP amplitude from aCSF to Mg²⁺ free was not
270 different when comparing the other experimental groups to control (**Figure 3B top**). However, the NMDAr
271 antagonist, AP5, reduced the fEPSP in 0-HIF1a^{+/-} and 10-HIF1a^{+/-} similar to that of control (**Figure 3A**,
272 red=AP5) yet was less effective in IH₁₀ (**Figure 3B bottom**). These findings suggested that IH suppressed

273 contribution of the conductance of NMDAr within neurons in a HIF1a dependent manner. Such an effect could
274 be due to direct effects on unitary conductance of the NMDAr or by the down regulation of the receptor itself.
275 Therefore, we examined whether expression of the GluN1, the obligatory subunit of the NMDAr, was disrupted
276 by IH.

277 We compared GluN1 subunit expression in control (n=5), IH₁₀ (n=5), 0-HIF1a^{+/-} (n=5) and 10-HIF1a^{+/-} (n=5). IH
278 reduced GluN1 in wildtype hippocampi, yet GluN1 expression was similar to control in both 0-HIF1a^{+/-} or 10-
279 HIF1a^{+/-} (**Figure 3C**). This reduction in NR1 may have resulted from an IH-mediated reduction in synapse.
280 Therefore, we sought to determine whether IH caused a reduction in a scaffolding protein of the glutamatergic
281 synapse PSD-95 (**Figure 3D**, n=3 per group). When compared to control, no difference in PSD-95 was
282 detected any experimental group (**Figure 3D**). These findings together indicated that IH-dependent HIF1a
283 signaling specifically likely targets a reduction of the NMDAr by suppressing GluN1 expression without
284 causing gross reductions in glutamatergic synapses. Such a reduction in NMDAr expression would likely
285 contribute to the reduced sensitivity to AP5 following IH and contribute to impaired NMDAr-dependent LTP.

286 As IH-dependent HIF1a signaling can lead to a pro-oxidant condition, we next sought to determine whether IH-
287 dependent HIF1a signaling enhanced ROS production within the hippocampus. Protein carbonyl content in
288 hippocampal homogenates from control (n=4), IH₁₀ (n=4), 0-HIF1a^{+/-} (n=4), and 10-HIF1a^{+/-} (n=4) revealed that
289 protein carbonyl content was elevated in IH₁₀ yet unchanged in homogenates from either 0-HIF1a^{+/-} or
290 10-HIF1a^{+/-} (**Figure 4A**). NADPH oxidase 4 (NOX4) is a ROS generating protein that can be transcriptionally
291 regulated by HIF1a (Diebold et al., 2010). Therefore, we next determined Nox4 expression in hippocampal
292 homogenates from control (n=5), IH₁₀ (n=5), 0-HIF1a^{+/-} (n=5), and 10-HIF1a^{+/-} (n=5). NOX4 was elevated in
293 IH₁₀ yet unchanged in homogenates from either 0-HIF1a^{+/-} or 10-HIF1a^{+/-} (**Figure 4B**). Together,
294 these data suggest that enhanced ROS production by IH-dependent HIF1a signaling involves the upregulation
295 of NOX4. However, IH-dependent ROS production was involved with the changed expression of GluN1
296 remained uncertain.

297 To resolve the involvement of IH-dependent ROS production on the regulation of GluN1, protein homogenates
298 were prepared from four groups: control (n=4); IH₁₀ (n=4); wildtype mice administered saline during ten days of
299 IH exposure (IH_{Saline}, n=4), wildtype mice administered, the superoxide anion scavenger, MnTMPyP during IH

300 (IH_{MnTMPyP}, n=4). GluN1 was reduced in IH₁₀ and IH_{Saline}; whereas, GluN1 from 10-MnTMPyP was similar to that
301 of control (**Figure 5A**), which coincided with the ability to evoke LTP_{TBS} from IH_{MnTMPyP} (n=5, **Figure 5B**).
302 Behavioral performance was also assessed in IH_{Saline} (n=11) and IH_{MnTMPyP} (n=10). Both IH_{Saline} and IH_{MnTMPyP}
303 exhibited an progressive improvement in locating the exit as indicated by the total latency to exit over the
304 course of training (**Figure 5C**). During the probe trial, the two groups exhibited similar values for distance to
305 initial entry into the exit zone (IH_{Saline} = 0.29 ± 0.06 m, IH_{MnTMPyP} = 0.28 ± 0.05 m; P=0.87, data not shown), and
306 similar latency to initial entry into the exit zone (IH_{Saline} = 77.74 ± 24.42 sec, IH_{MnTMPyP} = 26.00 ± 5.67 sec;
307 P=0.06, data not shown), although the variance between the values for latency to initial entry were different
308 between IH_{Saline} and IH_{MnTMPyP} (F=17.00, DFn=10, Dfd=11; P<0.0001; data not shown). Moreover, entry
309 probability into the exit zone during the probe trial was greater in IH_{MnTMPyP} (**Figure 5D**, IH_{Saline} = 4.33 ± 0.63%,
310 IH_{MnTMPyP} = 10.32 ± 1.26%; P=0.0005). These data indicated that scavenging IH-derived superoxide anion
311 prevented the reduction in the obligatory subunit of the NMDAr, prevented the loss of LTP_{TBS}, and mitigated
312 behavioral deficits caused by IH.

313 Discussion

314 Our study establishes a role for IH-dependent HIF1a signaling in impairing hippocampal neurophysiology that
315 supports spatial memory. Consistent with previous reports indicating that IH impacts spatial memory (Row et
316 al., 2002; Gozal et al., 2003), we observed that IH disrupted performance in the Barnes maze. The cognitive
317 disruptions we observed coincided with enhanced nuclear HIF1a in the hippocampus, a shift toward a pro-
318 oxidant state, and impairment to NMDAr-dependent LTP. We found that either heterozygosity in HIF1a and
319 antioxidant administration prevented the effects of IH on the hippocampus. Together these findings reveal a
320 mechanistic pathway by which IH such as that experienced with sleep apnea impairs mechanisms
321 underpinning spatial memory.

322 Evaluating the behavioral performance in Control and IH₁₀, showed that both groups progressively improved
323 with training, yet prominent differences were present during the probe trial. These results suggested IH
324 produced modest impairments to cognitive performance and is reminiscent of mild cognitive deficits
325 documented among individuals suffering from sleep apnea (Wallace and Bucks, 2013; Devita et al., 2017b;
326 Leng et al., 2017). These behavioral impairments coincided with targeted loss in NMDAr-dependent LTP after

327 IH. However, neither the behavioral deficits nor impaired synaptic potentiation was observed in HIF1a^{+/-}
328 exposed to IH implicating a role for IH-dependent HIF1a signaling in these phenomena.

329 Although administration of the prolyl hydroxylase inhibitor, Dimethylxalylglycine (DMOG), enhances HIF1a
330 and coincides with the suppression of hippocampal LTP (Wall et al., 2014), this pharmacological approach for
331 enhancing HIF1a, can also disrupt cellular respiration well-before the activation of HIF1a dependent pathways
332 (Zhdanov et al., 2015). This confounds understanding how enhanced HIF1a may impact hippocampal synaptic
333 plasticity. Our experiments using HIF1a^{+/-} mice resolved this issue. Heterozygosity in HIF1a prevented the IH-
334 dependent increase in NOX4, the ROS producing enzyme transcriptionally regulated by HIF1a (Diebold et al.,
335 2010). Increasing NOX4 would be expected to increase the production of ROS, and if left unchecked promote
336 a pro-oxidant state. Indeed, IH led to increased protein carbonylation, an indication of a shift toward a more
337 pro-oxidant state. The HIF1a dependent increase in pro-oxidant condition was presumably due to ROS
338 production from the enhanced presence of NOX4. The pro-oxidant state suppressed NMDAr-dependent LTP
339 and disrupted performance in the Barnes maze.

340 In agreement with a previous report (Gozal et al., 2001), our protein analyses indicated that IH reduced GluN1
341 expression, the obligatory subunit of the NMDAr. Alone, this observation could not discriminate whether the
342 effect of IH on GluN1 expression reflected a reduction of the NMDAr at the glutamatergic synapse, a decline in
343 extrasynaptic receptors, a premature degradation of GluN1 prior to assembly of the receptor or some
344 combination of the three. The reduction in GluN1 was not accompanied by a reduction in PSD-95 suggesting
345 that IH did not indiscriminately cause a loss of glutamatergic synapses. Following IH, the unpotentiated fEPSP
346 (in Mg²⁺ free aCSF) was less sensitive to NMDAr blockade. Together these findings may be interpreted as
347 indicating that IH remodels the glutamatergic synapse by reducing receptor expression. Such a reduction in
348 the synaptic NMDAr would likely disrupt NMDAr-dependent LTP. However, this may not be the only avenue by
349 which IH disturbs NMDAr-based physiology.

350 Administration of MnTMPyP during IH prevented both GluN1 reduction and impairment to NMDAr dependent
351 LTP. Similarly, in 10-HIF1a^{+/-}, GluN1 expression and NMDAr-dependent LTP was similar to that of control.
352 These findings together indicate that HIF1a mediated ROS production is a principal mechanism that diminishes
353 NMDAr function. While our experiments support the possibility that IH causes reduced receptor expression, the

354 conductance of the NMDAr is known to be redox sensitive (Bodhinathan et al., 2010; Kumar and Foster, 2013).
355 Specifically, oxidation of the NMDAr attenuates NMDAr conductance (Choi and Lipton, 2000; Lipton et al.,
356 2002; Guidi et al., 2015; Foster et al., 2017). It is, therefore, likely that some combination of oxidative
357 modulation and downregulation of the NMDAr mediates the disrupted NMDAr physiology caused by IH.
358 However, we did not acutely manipulate redox state and do not know to what extent the two processes
359 contribute IH-dependent effects on NMDAr activity. This remains an open question to be investigated.

360 Independent of the precise cause, changed NMDAr activity by IH likely decreases the NMDAr-dependent rise
361 in intracellular Ca^{2+} . While a rise intracellular Ca^{2+} is an important event for downstream intracellular signaling
362 critical to LTP, it also is likely to mediate other Ca^{2+} -dependent processes within the neuron. With respect to
363 IH, ROS production can increase intracellular Ca^{2+} via the Inositol 1,4,5-trisphosphate receptor (IP3R) (Yuan et
364 al., 2008), which then serves as a positive feedback mechanism to enhance and stabilize HIF1a signaling
365 (Prabhakar and Semenza, 2012). As we observed that IH increases NOX4 and protein carbonyls in a HIF1a
366 dependent fashion, excess elevations in intracellular Ca^{2+} within hippocampal cells may promote a feedforward
367 mechanism that enhances HIF1a activity and ROS generation. Thus, the reduction of NMDAr activity may
368 serve as a necessary phenomenon to minimize intracellular Ca^{2+} and prevent potential exacerbation of cellular
369 stress if left unregulated.

370 The forced shift from NMDAr-dependent to NMDAr-independent forms of synaptic plasticity observed with IH is
371 a phenomenon also found in models of the aging (Boric et al., 2008; Robillard et al., 2011). Thus, IH, like
372 normal aging, limits the mechanisms normally used to support learning and memory in younger animals. Our
373 work indicates that the HIF1a dependent pro-oxidant condition causes this aging phenotype. As the current
374 study used younger animals (P50-P80), examining how IH affects mechanisms of learning and memory in
375 aged subjects will be important to resolve.

376 In conclusion, we have identified an important pathway by which IH-dependent HIF1a signaling causes a
377 pro-oxidant state that destabilizes hippocampal synaptic plasticity and disrupts spatial memory. We propose
378 that these observations establish a mechanistic framework by which sleep apnea may lower of the threshold
379 for cognitive impairment (**Figure 6**). This mechanism may contribute to the emergence of neurological
380 diseases associated with untreated sleep apnea.

382 **Table 1. Description of statistical tests and associated values used throughout the study.**

383 **Figure 1. Ten days of IH increases hippocampal hypoxia inducible factor 1a (HIF1a) and disrupts**
384 **Barnes maze performance in wild type mice but not in HIF1a^{+/-}.** **A. Left:** Representative digitized western
385 blot images for HIF1a (103 kDa) and PCNA, (40 kDa) in hippocampal nuclear protein fractions from control
386 (n=4) and IH₁₀ (n=4). **Right:** Quantification of HIF1a protein normalized to PCNA revealed that nuclear HIF1a
387 was increased in IH₁₀ when compared to control (P=0.019). **B.** Total latency to exit the Barnes maze during
388 three training sessions in control (n=10) and in IH₁₀ (n=11). Each blue (control) and red (IH₁₀) line represents
389 an individual performance during training. Training to the exit was conducted over three sessions. Each
390 session was separated by 24 hours. **C. Right:** During the probe trial, the distance traveled to initially enter the
391 exit zone was shorter in Control when compared to IH₁₀ (P=0.048). **Right:** Latency to initial entry was smaller in
392 control as well (P=0.034). **D.** Heat maps of the mean entry probability across all false exits (1 to 19) and the
393 exit zone during probe trial for the control and IH₁₀. Comparison of entry probability into the exit zone during the
394 probe trial reveals that control has a greater probability for entering the exit zone when compared to IH₁₀
395 (P=0.004). **E. Left:** Representative digitized western blot images HIF1a and PCNA in hippocampal nuclear
396 protein fractions from 0-HIF1a^{+/-} (n=4) and 10-HIF1a^{+/-} (n=4). **Right:** Quantification of HIF1a protein normalized
397 to PCNA revealed that nuclear HIF1a is similar between 0-HIF1a^{+/-} and 10-HIF1a^{+/-} (P=0.84). **F.** Total latency
398 to exit the Barnes maze during three training sessions in 0-HIF1a^{+/-} (n=7) and in 10-HIF1a^{+/-} (n=8). Each gray
399 (0-HIF1a^{+/-}) and yellow (10-HIF1a^{+/-}) line represents an individual performance during training. All experimental
400 groups exhibit decreased total latency over the course of training. **G. Left:** In HIF1a^{+/-}, the distance initial to
401 initial entry into the exit zone was similar between 0-HIF1a^{+/-} and 10-HIF1a^{+/-} (P=0.55). **Right:** Latency to initial
402 entry into the exit zone (E) during the probe trial were similar between 0-HIF1a^{+/-} and 10-HIF1a^{+/-} (P=0.39).
403 Heat maps of the mean entry probability into all zones during the probe trial for 0-HIF1a^{+/-} and 10-HIF1a^{+/-}.
404 Entry probability was similar between 0-HIF1a^{+/-} and 10-HIF1a^{+/-} (P=0.21). * = P < 0.05; ** = P < 0.01; N.S. = P > 0.05.

405

406 **Figure 2. IH suppresses NMDAr-dependent synaptic potentiation in wildtype hippocampal slices, but**
407 **NMDAr-dependent LTP is unaffected by IH in the hippocampal slices from HIF1a^{+/-}.** **A.** LTP was evoked

408 using high frequency stimulation (HFS) in control (blue, n=6) is attenuated by AP5 (green, n=5). LTP_{HFS} is
409 attenuated in following IH (IH₁₀, red, n=6) and is no longer sensitive to AP5 (IH+AP5, gold, n=5). A comparison
410 of LTP_{HFS} magnitude (60 min following HFS) was performed to compare experimental conditions to control.
411 **=P<0.01 **B.** LTP_{TBS} is readily evoked in control (light blue, n=5) and is completely blocked by AP5 (light
412 green, n=5). Following IH, LTP_{TBS} is present (IH₁₀, pink, n=5). Following a one-way ANOVA, a posthoc
413 comparison of LTP_{TBS} magnitude (60 min following TBS) was performed to compare experimental conditions to
414 control. ***=P<0.01 **C.** LTP_{HFS} was evoked in both 0-HIF1a^{+/-} (n=8, grey) and 10-HIF1a^{+/-} (n=8, dark yellow).
415 No difference was found when comparing LTP_{HFS} magnitude between 0-HIF1a^{+/-} and 10-HIF1a^{+/-} (P=0.94). **D.**
416 LTP_{TBS} was evoked in both 0-HIF1a^{+/-} (n=6, light grey), 10-HIF1a^{+/-} (n=5, light yellow) and 10-HIF1a^{+/-} + AP5
417 (n=5, light green). No difference was found when comparing LTP_{TBS} magnitude of 0-HIF1a^{+/-} and 10-HIF1a^{+/-}.
418 Representative traces illustrate baseline (black) and 60 mins following HFS (colored trace). Scale bars 0.2
419 mV/10 ms. In experiments using AP5, electrophysiological recordings began at 20 min prior to eliciting LTP
420 (i.e., t=-20) while AP5 was applied 10 prior to eliciting LTP (i.e., t=-10). For all the experiment, the arrow
421 represents the electric protocols: HFS or TBS.***P<0.001; **P=<0.01; N.S.=P>0.05.

422

423 **Figure 3. The IH reduces the contribution of the NMDAr to fEPSP and GluN1 protein from wildtype mice**
424 **but does not induce these changes in HIF1a^{+/-}.** **A.** Representative traces of the fEPSP from control, IH₁₀, 0-
425 HIF1a^{+/-} and 10-HIF1a^{+/-} in: aCSF (black), Mg²⁺free media (blue) and Mg²⁺free media with AP5 (red). Scale
426 bars: 0.4 mV/10 ms). **B. Top:** Change in amplitude of the fEPSP from aCSF to Mg²⁺free media. **Bottom:**
427 Change in amplitude of the fEPSP from Mg²⁺free media to Mg²⁺free media with AP5. *P=<0.05; N.S.=P>0.05.
428 **C. Left:** Representative western blots of GluN1 and the housekeeping protein, GAPDH from control (n=5), IH₁₀
429 (n=5), 0-HIF1a^{+/-} (n=5), and 10-HIF1a^{+/-} (n=5). **Right:** Comparisons of normalized GluN1 protein expression
430 was performed to compare experimental conditions to control. This revealed that GluN1 was reduced in IH₁₀
431 and unchanged in both 0-HIF1a^{+/-} and 10-HIF1a^{+/-}. *P<0.05; N.S.=P>0.05. **D. Left:** Representative western
432 blots of PSD-95 and the housekeeping protein, GAPDH from control (n=3), IH₁₀ (n=3), 0-HIF1a^{+/-} (n=3), and

433 10-HIF1a^{+/-} (n=3). *Right*: Comparisons of normalized PSD-95 protein expression was performed to compare
434 experimental conditions to control. *=P<0.05; N.S.=P>0.05.

435 **Figure 4. IH enhances protein carbonyl content and increase NOX4 expression in wildtype but not in**
436 **HIF1a^{+/-}. A.** Hippocampal homogenates from control (n=4), IH₁₀ (n=4), 0-HIF1a^{+/-} (n=4), and 10-HIF1a^{+/-} (n=4).
437 While IH10 displayed elevated protein carbonyl content was not elevated in either 0-HIF1a^{+/-} or 10-HIF1a^{+/-}. **B.**
438 Comparison of the pro-oxidant enzyme, NOX4, from control (n=5), IH₁₀ (n=5), 0-HIF1a^{+/-} (n=5) and 10-HIF1a^{+/-}
439 (n=5) reveals that NOX4 is increased in IH₁₀; P<0.01), but not elevated in either 0-HIF1a^{+/-} or 10-HIF1a^{+/-}.
440 **=P<0.01; N.S.=P>0.05.

441 **Figure 5. Antioxidant treatment mitigates the IH-dependent effects on GluN1 expression, LTP_{TBS}, and**
442 **performance in the Barnes maze. A. Left:** Representative western blots of GluN1 and GAPDH from Control,
443 IH₁₀, wildtype mice treated with saline during ten days of IH (*i.e.*, vehicle control exposed to IH, IH_{Saline}, n=4),
444 wildtype mice treated with MnTMPyP during ten days of IH (IH_{MnTMPyP}). *Right*: Normalized GluN1 protein
445 expression was examined in control (n=4), IH₁₀ (n=4), IH_{Saline} (n=4), IH_{MnTMPyP} (n=4). No difference in GluN1
446 was evident between IH₁₀ (open black circles in IH₁₀ label) and IH_{Saline}, (open blue circles in IH₁₀ label);
447 therefore, the two groups were merged into the IH₁₀ label for comparisons to control. Comparisons revealed
448 that GluN1 was reduced only in IH₁₀ and unchanged in IH_{MnTMPyP}. **B.** In hippocampal slices from IH_{MnTMPyP},
449 LTP_{TBS} (n=5) could be reliably evoked contrasting the effect of IH₁₀ on LTP_{TBS} (see Figure 2B) Scale bars: 0.2
450 mV/10 ms. The arrow represent the TBS protocol. **C.** The total latency to exit the Barnes maze progressively
451 decreased in both IH_{Saline} (n=11, pink lines represent individual performance) and IH_{MnTMPyP} (n=10, purple lines
452 represent individual performance) suggesting that both groups could learn the exit zone location. **D.** Heat maps
453 of the mean entry probability across all false exits (1 to 19) and the exit zone during the probe trial for IH_{Saline}
454 and IH_{MnTMPyP}. Comparison of entry probability into the exit zone during the probe trial reveals that IH_{MnTMPyP}
455 has a greater probability for entering the exit zone when compared to IH_{Saline} (P=0.006). ***P=<0.001;
456 *=P<0.05; N.S.=P>0.05.

457 **Figure 6. A mechanistic framework by which sleep apnea lowers the threshold for cognitive**
458 **impairment.** Schematic synthesizing our findings into a pathway by which intermittent hypoxia (IH) promotes a
459 pro-oxidant state in the hippocampus that impairs NMDAr-dependent plasticity and spatial memory.

460

461 **References**

- 462 Bodhinathan K, Kumar A, Foster TC (2010) Intracellular redox state alters NMDA receptor response during
463 aging through Ca²⁺/calmodulin-dependent protein kinase II. *The Journal of neuroscience : the official*
464 *journal of the Society for Neuroscience* 30:1914-1924.
- 465 Boric K, Munoz P, Gallagher M, Kirkwood A (2008) Potential adaptive function for altered long-term
466 potentiation mechanisms in aging hippocampus. *The Journal of neuroscience : the official journal of the*
467 *Society for Neuroscience* 28:8034-8039.
- 468 Cha J, Zea-Hernandez JA, Sin S, Graw-Panzer K, Shifteh K, Isasi CR, Wagshul ME, Moran EE, Posner J,
469 Zimmerman ME, Arens R (2017) The Effects of Obstructive Sleep Apnea Syndrome on the Dentate
470 Gyrus and Learning and Memory in Children. *The Journal of neuroscience : the official journal of the*
471 *Society for Neuroscience* 37:4280-4288.
- 472 Choi YB, Lipton SA (2000) Redox modulation of the NMDA receptor. *Cellular and molecular life sciences :*
473 *CMLS* 57:1535-1541.
- 474 Chou YT, Zhan G, Zhu Y, Fenik P, Panossian L, Li Y, Zhang J, Veasey S (2013) C/EBP homologous binding
475 protein (CHOP) underlies neural injury in sleep apnea model. *Sleep* 36:481-492.
- 476 Christakis DA, Ramirez JS, Ramirez JM (2012) Overstimulation of newborn mice leads to behavioral
477 differences and deficits in cognitive performance. *Scientific reports* 2:546.
- 478 Devita M, Montemurro S, Ramponi S, Marvisi M, Villani D, Raimondi MC, Rusconi ML, Mondini S (2017a)
479 Obstructive sleep apnea and its controversial effects on cognition. *Journal of clinical and experimental*
480 *neuropsychology* 39:659-669.
- 481 Devita M, Montemurro S, Zangrossi A, Ramponi S, Marvisi M, Villani D, Raimondi MC, Merlo P, Rusconi ML,
482 Mondini S (2017b) Cognitive and motor reaction times in obstructive sleep apnea syndrome: A study
483 based on computerized measures. *Brain and cognition* 117:26-32.
- 484 Diebold I, Petry A, Hess J, Gorlach A (2010) The NADPH oxidase subunit NOX4 is a new target gene of the
485 hypoxia-inducible factor-1. *Molecular biology of the cell* 21:2087-2096.
- 486 Foster TC, Kyritsopoulos C, Kumar A (2017) Central role for NMDA receptors in redox mediated impairment of
487 synaptic function during aging and Alzheimer's disease. *Behavioural brain research* 322:223-232.
- 488 Gildeh N, Drakatos P, Higgins S, Rosenzweig I, Kent BD (2016) Emerging co-morbidities of obstructive sleep
489 apnea: cognition, kidney disease, and cancer. *Journal of thoracic disease* 8:E901-E917.
- 490 Goldbart A, Cheng ZJ, Brittan KR, Gozal D (2003) Intermittent hypoxia induces time-dependent changes in the
491 protein kinase B signaling pathway in the hippocampal CA1 region of the rat. *Neurobiology of disease*
492 14:440-446.
- 493 Gozal D, Daniel JM, Dohanich GP (2001) Behavioral and anatomical correlates of chronic episodic hypoxia
494 during sleep in the rat. *The Journal of neuroscience : the official journal of the Society for Neuroscience*
495 21:2442-2450.
- 496 Gozal D, Row BW, Gozal E, Kheirandish L, Neville JJ, Brittan KR, Sachleben LR, Jr., Guo SZ (2003)
497 Temporal aspects of spatial task performance during intermittent hypoxia in the rat: evidence for
498 neurogenesis. *The European journal of neuroscience* 18:2335-2342.

- 499 Guidi M, Kumar A, Foster TC (2015) Impaired attention and synaptic senescence of the prefrontal cortex
500 involves redox regulation of NMDA receptors. *The Journal of neuroscience : the official journal of the*
501 *Society for Neuroscience* 35:3966-3977.
- 502 Iyer NV, Kotch LE, Agani F, Leung SW, Laughner E, Wenger RH, Gassmann M, Gearhart JD, Lawler AM, Yu
503 AY, Semenza GL (1998) Cellular and developmental control of O₂ homeostasis by hypoxia-inducible
504 factor 1 alpha. *Genes & development* 12:149-162.
- 505 Khuu MA, Pagan CM, Nallamotheu T, Hevner RF, Hodge RD, Ramirez JM, Garcia AJ, 3rd (2019) Intermittent
506 Hypoxia Disrupts Adult Neurogenesis and Synaptic Plasticity in the Dentate Gyrus. *The Journal of*
507 *neuroscience : the official journal of the Society for Neuroscience* 39:1320-1331.
- 508 Kumar A, Foster TC (2013) Linking redox regulation of NMDAR synaptic function to cognitive decline during
509 aging. *The Journal of neuroscience : the official journal of the Society for Neuroscience* 33:15710-
510 15715.
- 511 Leng Y, McEvoy CT, Allen IE, Yaffe K (2017) Association of Sleep-Disordered Breathing With Cognitive
512 Function and Risk of Cognitive Impairment: A Systematic Review and Meta-analysis. *JAMA neurology*
513 74:1237-1245.
- 514 Lipton SA, Choi YB, Takahashi H, Zhang D, Li W, Godzik A, Bankston LA (2002) Cysteine regulation of protein
515 function--as exemplified by NMDA-receptor modulation. *Trends in neurosciences* 25:474-480.
- 516 Macey PM, Prasad JP, Ogren JA, Moiyadi AS, Aysola RS, Kumar R, Yan-Go FL, Woo MA, Albert Thomas M,
517 Harper RM (2018) Sex-specific hippocampus volume changes in obstructive sleep apnea. *NeuroImage*
518 *Clinical* 20:305-317.
- 519 Nair D, Dayyat EA, Zhang SX, Wang Y, Gozal D (2011) Intermittent hypoxia-induced cognitive deficits are
520 mediated by NADPH oxidase activity in a murine model of sleep apnea. *PloS one* 6:e19847.
- 521 Payne RS, Goldbart A, Gozal D, Schurr A (2004) Effect of intermittent hypoxia on long-term potentiation in rat
522 hippocampal slices. *Brain research* 1029:195-199.
- 523 Peng YJ, Prabhakar NR (2003) Reactive oxygen species in the plasticity of respiratory behavior elicited by
524 chronic intermittent hypoxia. *Journal of applied physiology* 94:2342-2349.
- 525 Peng YJ, Yuan G, Ramakrishnan D, Sharma SD, Bosch-Marce M, Kumar GK, Semenza GL, Prabhakar NR
526 (2006) Heterozygous HIF-1alpha deficiency impairs carotid body-mediated systemic responses and
527 reactive oxygen species generation in mice exposed to intermittent hypoxia. *The Journal of physiology*
528 577:705-716.
- 529 Prabhakar NR, Semenza GL (2012) Adaptive and maladaptive cardiorespiratory responses to continuous and
530 intermittent hypoxia mediated by hypoxia-inducible factors 1 and 2. *Physiological reviews* 92:967-1003.
- 531 Robillard JM, Gordon GR, Choi HB, Christie BR, MacVicar BA (2011) Glutathione restores the mechanism of
532 synaptic plasticity in aged mice to that of the adult. *PloS one* 6:e20676.
- 533 Row BW, Kheirandish L, Neville JJ, Gozal D (2002) Impaired spatial learning and hyperactivity in developing
534 rats exposed to intermittent hypoxia. *Pediatric research* 52:449-453.
- 535 Semenza GL, Prabhakar NR (2015) Neural regulation of hypoxia-inducible factors and redox state drives the
536 pathogenesis of hypertension in a rodent model of sleep apnea. *Journal of applied physiology*
537 119:1152-1156.

- 538 Sforza E, Celle S, Saint-Martin M, Barthelemy JC, Roche F (2016) Hippocampus volume and subjective
539 sleepiness in older people with sleep-disordered breathing: a preliminary report. *Journal of sleep*
540 *research* 25:190-193.
- 541 Song X, Roy B, Kang DW, Aysola RS, Macey PM, Woo MA, Yan-Go FL, Harper RM, Kumar R (2018) Altered
542 resting-state hippocampal and caudate functional networks in patients with obstructive sleep apnea.
543 *Brain and behavior* 8:e00994.
- 544 Varga AW, Kishi A, Mantua J, Lim J, Koushyk V, Leibert DP, Osorio RS, Rapoport DM, Ayappa I (2014)
545 Apnea-induced rapid eye movement sleep disruption impairs human spatial navigational memory. *The*
546 *Journal of neuroscience : the official journal of the Society for Neuroscience* 34:14571-14577.
- 547 Wall AM, Corcoran AE, O'Halloran KD, O'Connor JJ (2014) Effects of prolyl-hydroxylase inhibition and chronic
548 intermittent hypoxia on synaptic transmission and plasticity in the rat CA1 and dentate gyrus.
549 *Neurobiology of disease* 62:8-17.
- 550 Wallace A, Bucks RS (2013) Memory and obstructive sleep apnea: a meta-analysis. *Sleep* 36:203-220.
- 551 Xie H, Leung KL, Chen L, Chan YS, Ng PC, Fok TF, Wing YK, Ke Y, Li AM, Yung WH (2010) Brain-derived
552 neurotrophic factor rescues and prevents chronic intermittent hypoxia-induced impairment of
553 hippocampal long-term synaptic plasticity. *Neurobiology of disease* 40:155-162.
- 554 Yuan G, Nanduri J, Khan S, Semenza GL, Prabhakar NR (2008) Induction of HIF-1alpha expression by
555 intermittent hypoxia: involvement of NADPH oxidase, Ca²⁺ signaling, prolyl hydroxylases, and mTOR.
556 *Journal of cellular physiology* 217:674-685.
- 557 Zhang SX, Wang Y, Gozal D (2012) Pathological consequences of intermittent hypoxia in the central nervous
558 system. *Comprehensive Physiology* 2:1767-1777.
- 559 Zhdanov AV, Okkelman IA, Collins FW, Melgar S, Papkovsky DB (2015) A novel effect of DMOG on cell
560 metabolism: direct inhibition of mitochondrial function precedes HIF target gene expression. *Biochimica*
561 *et biophysica acta* 1847:1254-1266.

562

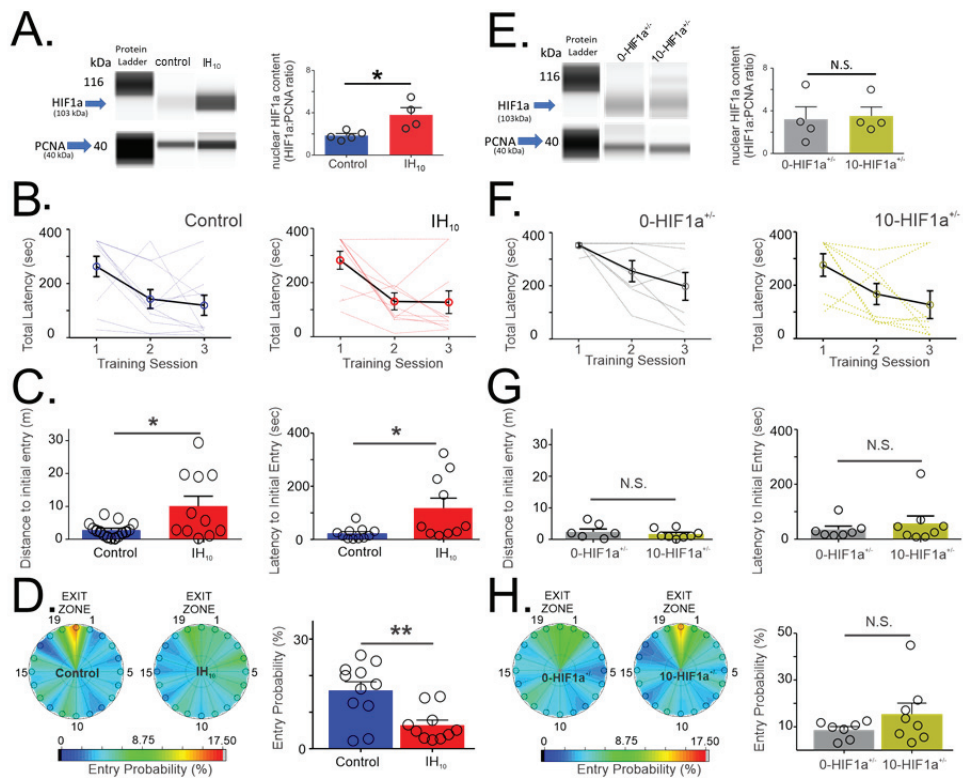
563

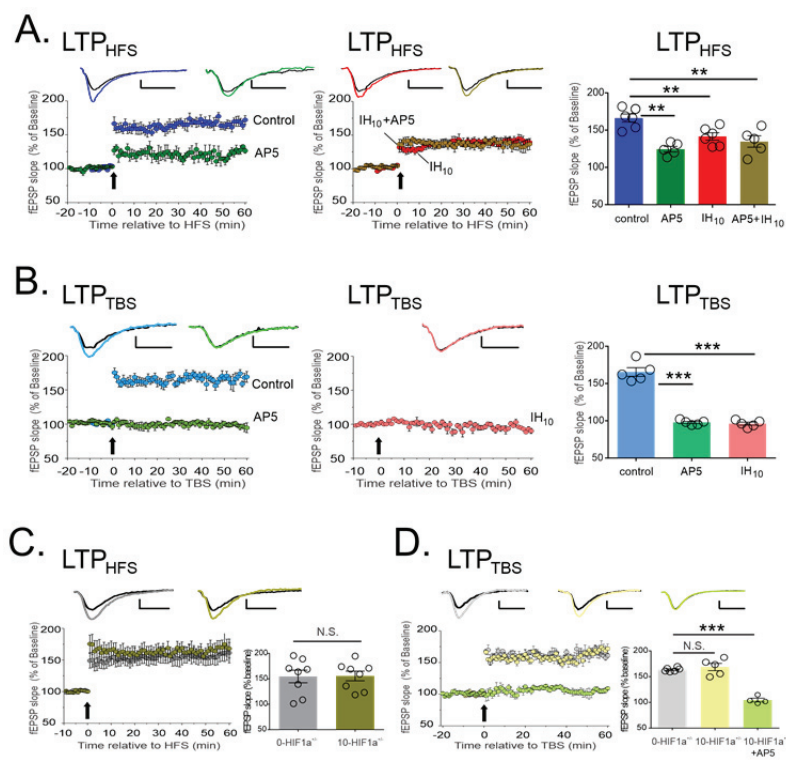
Table 1

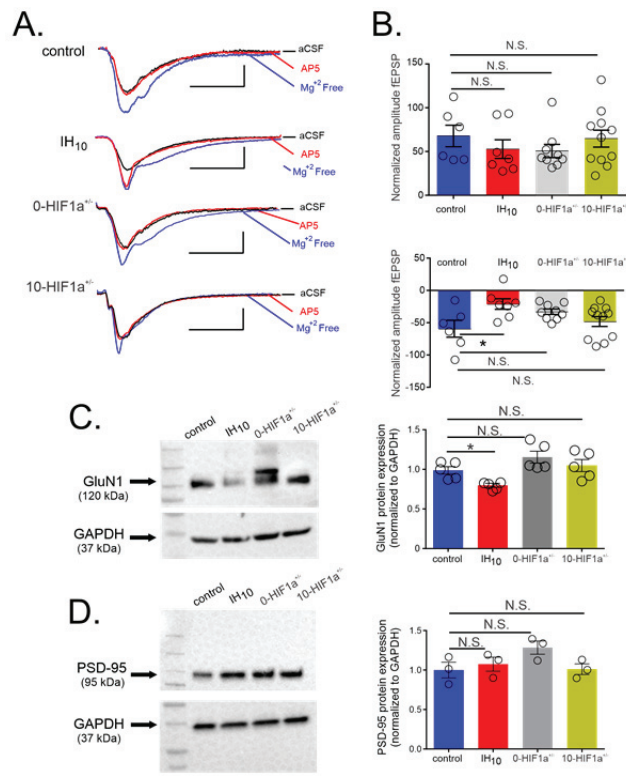
Figure	Statistical test	Statistical Values
1A	Unpaired t test with Welch's correction	P=0.03; t=2.789, df=3
1B (left)	one-way ANOVA, Dunnett's multiple comparison test	one-way ANOVA P=0.0044, F=7.191, 1 vs. 2 (training session): P<0.05, CI of diff=-23.74 to 217.9; 1 vs. 3 (training session): P<0.01, CI of diff 47.11 to 241.3
1B (right)	one-way ANOVA, Dunnett's multiple comparison test.	one-way ANOVA P=0.0006, F=11.68, 1 vs. 2 (training session): P<0.01, CI of diff=-63.81 to 239.3; 1 vs. 3 (training session): P<0.001, CI of diff 66.88 to 242.3
1C (left)	Unpaired t test with Welch's correction	P=0.04, t=2.85, df=9
1C (right)	Unpaired t test with Welch's correction	P=0.03, t=2.501, df=9
1D	Unpaired t test with Welch's correction	P=0.0037; t=3.436, df=15
1E	Unpaired t test with Welch's correction	P=0.84; t=0.2118, df=5
1F (left)	one-way ANOVA, Dunnett's multiple comparison test	one-way ANOVA P=0.0136, F=6.288, 1 vs. 2 (training session): P>0.05, CI of diff=-12.74 to 207.3; 1 vs. 3 (training session): P<0.01, CI of diff=44.13 to 264.2
1F (right)	one-way ANOVA, Dunnett's multiple comparison test	one-way ANOVA P=0.0156, F=5.688, 1 vs. 2 (training session): P>0.05, CI of diff=-3.202 to 221.3; 1 vs. 3 (training session): P<0.05, CI of diff=36.56 to 261.1
1G (left)	Unpaired t test with Welch's correction	P=0.547, t=0.6258, df=9
1G (right)	Unpaired t test with Welch's correction	P=0.48, t=0.7431, df=9

1H (left)	Unpaired t test with Welch's correction	P=0.2120, t=1.356, df=8
2A	one-way ANOVA, Dunnett's multiple comparison test	one way ANOVA P=0.0004, F=10.20; control vs.AP5: P<0.01, CI of diff=21.28 to 62.13; control vs.10IH: P<0.01, CI of diff=5.21 to 44.71; control vs.10-IH+AP5: P<0.01, CI of diff=11.04 to 51.89
2B	one-way ANOVA, Dunnett's multiple comparison test	one-way ANOVA P<0.0001, F=116.9; control vs.AP5: P<0.01, CI of diff=54.80 to 80.72; control vs.10IH: P<0.01, CI of diff=56.41 to 82.32.
2C	Unpaired t test with Welch's correction	P=0.94; t=0.065, df=13.14
2D	one-way ANOVA, Dunnett's multiple comparison test	one-way ANOVA P<0.0001, F=54.50; 0-HIF1a+/- vs.10-HIF1a+/-: P>0.05, CI of diff=-20.49 to 10.15; 10-HIF1a+/- vs.10-HIF1a+/- + AP5: P<0.01, CI of diff=42.75 to 75.42.
3B (top)	one-way ANOVA, Dunnett's multiple comparison test	one way ANOVA P=0.56, F=0.70; control vs.IH10: P>0.05, CI of diff=-24.53 to 54.60; control vs.0-HIF1a+/-: P>0.05, CI of diff=-20.36 to 54.60; control vs.10-HIF1a+/-: P>0.05, CI of diff=-33.12 to 39.06
3B (bottom)	one-way ANOVA, Dunnett's multiple comparison test	one way ANOVA P=0.56, F=0.70; control vs.IH10: P<0.05, CI of diff=-70.53 to -6.241; control vs.0-HIF1a+/-: P>0.05, CI of diff=-56.75 to 3.840; control vs.10-HIF1a+/-: P>0.05, CI of diff=-40.38 to 17.97
3C	one-way ANOVA, Dunnett's multiple comparison test	one way ANOVA P=0.014, F=4.74; control vs.IH10: P<0.05, CI of diff=0.96 to 0.78 ; control vs.0-HIF1a+/-: P>0.05, CI of diff=-0.38 to 0.05; control vs.10-HIF1a+/-: P>0.05, CI of diff=-0.27 to 0.157
3D	one-way ANOVA, Dunnett's multiple comparison test	one way ANOVA P=0.14, F=2.39; control vs.IH10: P>0.05, CI of diff=-0.42 to 0.27 ; control vs.0-HIF1a+/-

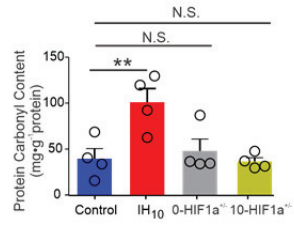
		: P>0.05, CI of diff=-0.63 to ;control vs.10-HIF1a+/-: P>0.05, CI of diff=-0.35 to 0.33
4A	one-way ANOVA, Dunnett's multiple comparison test	one way ANOVA P=0.006 F=6.871, control vs. IH10: P<0.01 CI of diff=-105.1 to -17.65; control vs. 0- HIF1a+/-: P>0.05 CI of diff=-52.12 to 35.32; control vs. 10-HIF1a+/-: P>0.05 CI of diff=-40.58 to 46.85
4B	one-way ANOVA, Dunnett's multiple comparison test	one way ANOVA P=0.003, F=11.70; control vs.IH10: P>0.05, CI of diff=-1.85 to -0.28 ; control vs.0- HIF1a+/-: P>0.05, CI of diff=-0.35 to 0.45 ;control vs.10-HIF1a+/-: P>0.05, CI of diff=-0.28 to 0.52
5A	one-way ANOVA, Dunnett's multiple comparison test	one-way ANOVA P=0.0023, F=10.00; control vs. IH10: P<0.01, CI of diff=0.09 to 0.75; control vs.10- MnTMPyP: P>0.05, CI of diff=-0.49 to 0.26
5B	one-way ANOVA, Dunnett's multiple comparison test	one-way ANOVA P<0.0001, F=57.60, control vs. IH: P<0.001, CI of diff= 50.58 to 88.15; control vs. IH+MnTMPyP: P>0.05, CI of diff -19.59 to 17.98
5C (Top)	one-way ANOVA, Dunnett's multiple comparison test	one-way ANOVA P=0.0008, F=6.32, 1 vs. 2 (training session): P>0.05, CI of diff=-40.99 to 139.5 ;1 vs. 3 (training session): P<0.001, CI of diff 71.59 to 252.1
5C (bottom)	one-way ANOVA, Dunnett's multiple comparison test	one-way ANOVA P=0.0056, F=9.10, 1 vs. 2 (training session): P>0.05, CI of diff=-25.40 to 187.3 ;1 vs. 3 (training session): P<0.01, CI of diff 55.75 to 268.4
5D	Unpaired t test with Welch's correction	P=0.0005; t=4.292, df=16.7112







A.



B.

